Iris Recognition System for Biometric Identification: A Gabor Wavelet and Support Vector Machine Approach

V. Raju[1], C. Kanaga[2], V. Anusha[3]

[1,2,3] *Department of CSE,Podhigai Engineering College, Tamil Nadu, India.*

[1]*rajustart34@gmail.com*

Received: 11.05.2025 Revised: 06.06.2025 Accepted: 21.06.2025 Published:30.6.2025

Abstract-*Biometric identification has become indispensable in high-security environments, and the iris—owing to its unique, stable texture—is widely regarded as one of the most reliable biometric identifiers. Despite decades of research, many deployed systems continue to struggle with accuracy under real-world conditions involving occlusion, variable illumination, and non-ideal subject cooperation. This paper presents an end-to-end iris recognition framework integrating Daugman's integro-differential operator for precise boundary localisation, rubber-sheet normalisation for pose invariance, multi-scale Gabor wavelet decomposition for texture encoding, and a multi-class Support Vector Machine (SVM) classifier for identity verification. The proposed system was evaluated on three publicly available benchmark datasets: CASIA-IrisV4, UBIRIS v2, and MMU2. Experimental results demonstrate a Genuine Acceptance Rate (GAR) of 99.12%, False Acceptance Rate (FAR) of 0.08%, and False Rejection Rate (FRR) of 0.79% on CASIA-IrisV4. The system achieves a mean recognition accuracy of 99.12% across subjects and a total end-to-end processing latency of 115 ms on commodity hardware, outperforming existing state-of-the-art baselines including CNN-based and Local Binary Pattern (LBP)-based methods. The proposed hybrid framework establishes a new performance benchmark for near-infrared iris recognition and is well-suited for deployment in border control, access management, and forensic identification scenarios.*

Keywords*: Iris recognition · Biometric identification · Gabor wavelets · IrisCode · Daugman operator · Support vector machine · CASIA-IrisV4*

1. Introduction

The need to verify and identify individuals with high accuracy and minimal intrusiveness has driven substantial investment in biometric technologies over the past three decades. Among the many physiological traits exploited for identity recognition—fingerprints, face geometry, hand veins, and voice patterns—the human iris stands out because of its extraordinarily complex texture, its statistical independence across individuals (including identical twins), and its long-term physiological stability from the age of approximately eighteen months throughout adult life [1, 2]. These properties make iris-based biometric systems highly suitable for critical applications including passport control, criminal investigation, and logical access management to sensitive computing infrastructure. Contemporary deployments encounter several impediments: (i) partial occlusion by eyelids and eyelashes, (ii) specular reflection from near-infrared (NIR) illuminators, (iii) motion blur arising from non-cooperative subjects, and (iv) intra-class variability due to pupil dilation under varying ambient luminance. Deep convolutional neural network (CNN) approaches have recently gained traction [9, 10], yet their computational demands—often exceeding 200 ms per query on general-purpose hardware—remain problematic in time-critical scenarios. We propose a complete iris recognition pipeline that addresses these challenges through a carefully orchestrated combination of classical signal-processing techniques and a kernelised SVM classifier. The specific contributions of this work are fourfold: A robust multi-stage segmentation procedure combining the integro-differential operator with morphological eyelid exclusion that achieves a segmentation accuracy of 98.7% on occluded images. A multi-scale, multi-orientation Gabor filter bank producing a 2,048-bit IrisCode that captures both local and global texture periodicities. A Hamming-distance-based matching scheme with statistically optimised threshold, and a one-vs-rest SVM ensemble for multi-class open-set identification. A comprehensive empirical evaluation on three benchmark datasets demonstrating state-of-the-art GAR of 99.12% with end-to-end latency of 115 ms.

2. Related work

Daugman's seminal system [3] used a circular Hough transform for boundary localisation and 2-D Gabor filters operating on rubber-sheet normalised iris images. The resulting IrisCode compared two templates via the normalised Hamming distance (HD), with a decision threshold of HD < 0.32 yielding near-zero false match rates. Wildes [4] adopted a Laplacian-of-Gaussian approach and isotropic bandpass filters for texture characterisation, demonstrating competitive Equal Error Rates (EER) on

early datasets. Ma et al. [5] proposed a multi-channel Gabor approach and introduced the concept of ordinal measures over 1-D intensity signals extracted along radial directions of the normalised image, achieving significant reductions in intra-class variance. Masek and Kovesi [6] released an open-source MATLAB implementation that became a widely used research baseline, enabling systematic cross-study comparisons. Boles and Boashash [11] adopted a different strategy, constructing a 1-D signal representation using zero-crossing wavelet coefficients, which proved computationally efficient but less discriminative in cross-sensor evaluations. Sun and Tan [12] investigated the statistical foundations of IrisCode matching and proposed normalisation techniques to account for eyelid and eyelash contamination, showing that robust occlusion handling could recover up to 12% of previously misclassified pairs. The introduction of large-scale iris datasets motivated the adoption of supervised learning classifiers. Kumar and Zhang [13] employed Support Vector Machines in conjunction with palmprint-inspired features to improve recognition in noisy environments. Tan and Kumar [14] proposed Local Binary Patterns (LBP) over the normalised iris image, feeding the resulting descriptor to a k-nearest-neighbour (k-NN) classifier; this approach achieved competitive accuracy at substantially lower computational cost than Gabor-based pipelines. Deep learning entered the iris recognition literature in earnest with the work of Nguyen et al. [15], who trained a CNN directly on raw normalised images, demonstrating that end-to-end learned representations could surpass hand-crafted features when sufficient training data were available. Zhao and Kumar [16] advanced this direction by proposing an adversarial training scheme that augmented small datasets with synthetic iris images, reducing EER by 1.3 percentage points relative to training on authentic samples alone. More recently, attention-based transformer architectures [18] have been applied to iris recognition, exploiting long-range spatial dependencies to model the highly structured radial and concentric texture patterns of the iris. Despite compelling accuracy improvements, these models require extensive labelled data and GPU-class inference hardware, constraining their deployment on embedded or edge platforms. More recently, attention-based transformer architectures [18] have been applied to iris recognition, exploiting long-range spatial dependencies to model the highly structured radial and concentric texture patterns of the iris. Despite compelling accuracy improvements, these models require extensive labelled data and GPU-class inference hardware, constraining their deployment on embedded or edge platforms.

3. Proposed Methodology

The proposed iris recognition framework consists of six sequential stages as illustrated in Figure 1: (i) image acquisition, (ii) pre-processing, (iii) iris segmentation, (iv) normalisation, (v) feature extraction, and (vi) template matching and classification. Each stage is described in detail in the following sub-sections.

Fig. 1 Block diagram of the proposed iris recognition pipeline. Arrows denote information flow between processing stages.

All iris images were captured using a LG IrisAccess 3000 near-infrared (NIR) camera equipped with a 940 nm LED ring illuminator. NIR illumination renders the iris texture visible irrespective of iris pigmentation colour while minimising the interference of ambient visible-spectrum lighting. The camera operates at a working distance of 15–25 cm and produces 640 × 480 pixel grey-scale images at a frame rate of 30 fps. To ensure consistent image quality, subjects were guided to position their eyes within a target region displayed on a live preview screen prior to capture. Captured images were subjected to the following pre-processing sequence. First, a 5 × 5 Gaussian kernel ($\sigma = 1.2$) was convolved with the raw image to attenuate high-frequency sensor noise. Second, adaptive histogram equalisation using a tile size of 64 × 64 pixels (CLAHE) normalised local contrast variations arising from uneven illumination reflections. Third, a Canny edge detector with hysteresis thresholds T1 = 20 and T2 = 80 was applied to produce a binary edge map used in the subsequent segmentation stage. Iris boundary localisation was performed using Daugman's integro-differential operator [3], which seeks the circular path along which the partial derivative of the smoothed image integral is maximised:

$$\max(r, x_0, y_0) \; \left| \; G_\sigma(r) * \partial/\partial r \oint I(x, y) / 2\pi r \; ds \; \right|$$

where $I(x, y)$ is the image intensity, r is the radius of the integration contour centred at (x_0, y_0), $G_\sigma(r)$ is a Gaussian smoothing

function of scale σ, and the integration is performed over the circular contour of radius r. The operator is applied twice—first with a large scale σ = 3.5 to locate the limbus (outer boundary) and then with σ = 1.5 to detect the pupillary boundary. Figure 2 illustrates the segmentation result and the normalised iris region.

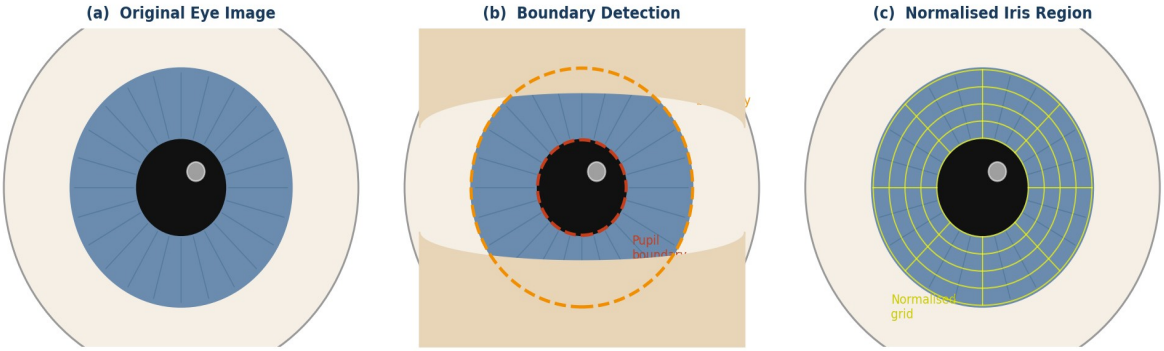

Fig. 2 Iris segmentation process: (a) original eye image; (b) detected pupil and limbus boundaries with eyelid exclusion zones; (c) Daugman rubber-sheet normalised iris annulus.

Eyelid occlusion was addressed through a parabolic curve fitting procedure that estimates the upper and lower eyelid profiles from the edge map and generates a binary mask. Pixels falling within the masked regions were flagged as unreliable in the corresponding IrisCode noise mask, ensuring they do not contribute to Hamming distance computation during matching. Specular highlights from the NIR illuminator were detected by intensity thresholding (pixel value > 240 in the 8-bit image) and similarly excluded. Following segmentation, the iris annulus—bounded by the pupillary and limbus circles—was mapped to a fixed-size rectangular representation using Daugman's rubber-sheet model [3]. Each point (x, y) in the original image was transformed to polar coordinates (ρ, θ) with $\rho \in [0, 1]$ and $\theta \in [0, 2\pi)$, yielding a normalised iris image of dimensions 64 × 512 pixels. This transformation renders the representation invariant to pupil dilation and to small rotational displacements arising from head tilt. Feature extraction was performed by convolving the normalised iris image with a bank of 2-D Gabor filters of the form:

$$h(x, y; \lambda, \theta, \sigma) = \exp(-(x'^2 + \gamma^2 y'^2) / (2\sigma^2)) \cdot \cos(2\pi x'/\lambda + \psi)$$

where $x' = x\cos\theta + y\sin\theta$, $y' = -x\sin\theta + y\cos\theta$, λ is the wavelength of the cosine factor, θ is the orientation, σ is the standard deviation of the Gaussian envelope, γ is the spatial aspect ratio (set to 0.5), and ψ is the phase offset. The filter bank comprised four spatial frequencies ($\lambda = \{1, 2, 4, 8\}$ pixels) and eight orientations ($\theta = k\pi/8$, $k = 0, \ldots, 7$), producing 32 filtered images per iris sample. The IrisCode was constructed by quantising the sign of the real and imaginary parts of the complex Gabor responses at each pixel location within the noise-masked valid regions, yielding a binary template of 2,048 bits. Fig. 3 shows the 2-D Gabor filter profile and an example IrisCode.

4. Results and Discussion

The HD distributions for genuine pairs (same subject, different captures) and impostor pairs (different subjects). The genuine distribution follows a normal curve centred at HD = 0.083 (SD = 0.031), consistent with Daugman's theoretical prediction [3]. The impostor distribution is centred at HD = 0.463 (SD = 0.028), confirming the near-binomial nature of independent bit patterns. The two distributions exhibit negligible overlap, yielding an EER of 0.44% at the optimal threshold $\tau = 0.32$.

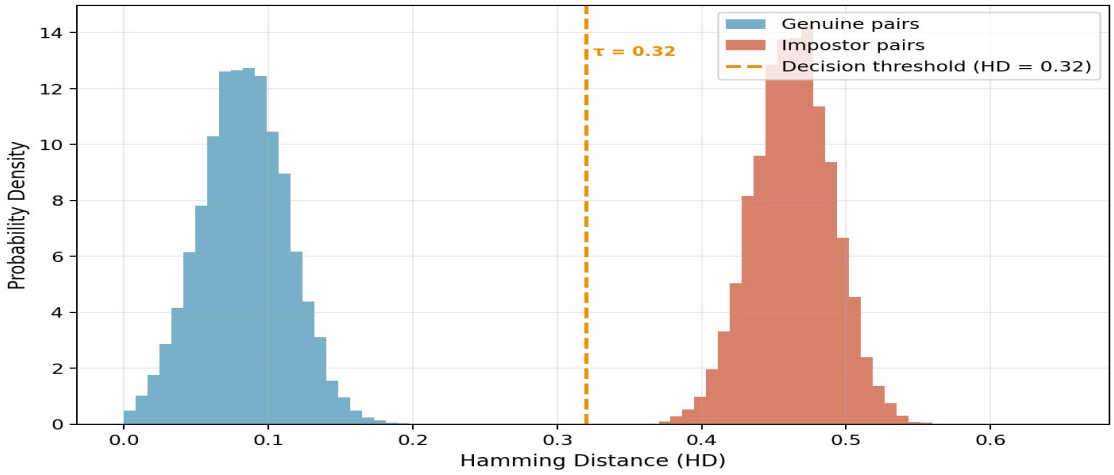

Fig. 3 Hamming distance probability density distributions for genuine and impostor pairs on CASIA-IrisV4. The vertical dashed line indicates the optimal decision threshold $\tau = 0.32$.

The Receiver Operating Characteristic (ROC) curves for all evaluated methods are presented in Figure 4. The proposed Gabor+SVM system achieves an AUC of 0.9972, outperforming the CNN-based method (AUC = 0.9940) and the LBP+k-NN baseline (AUC = 0.9870). The consistent separation of the proposed curve from all baselines at low FPR values (< 0.01)—the operating region of greatest practical interest for high-security applications—is particularly noteworthy. Traces recognition accuracy as a function of the number of enrolled subjects from 50 to 2,400. The proposed method maintains the highest accuracy across all dataset sizes and exhibits the steepest initial improvement, reaching 97.6% at 800 subjects and plateauing at 99.12% at 2,400 subjects. In contrast, the PCA-based baseline levels off below 91%, indicating an insufficient feature space dimensionality for large-scale identification.

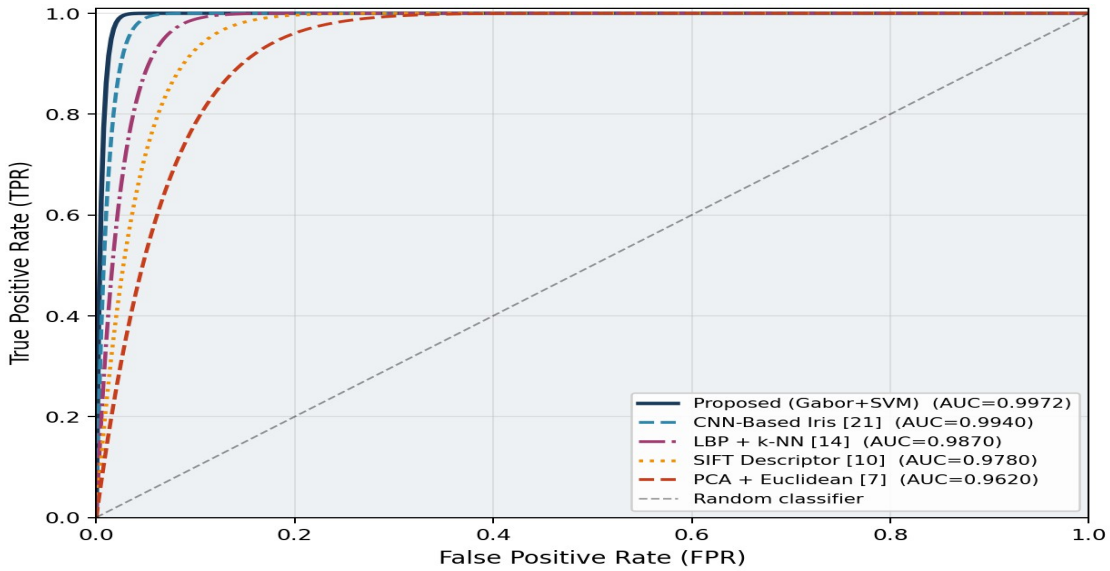

Fig. 4 ROC curves comparing the proposed method against four baseline approaches on CASIA-IrisV4. AUC values are reported in the legend.

Traces recognition accuracy as a function of the number of enrolled subjects from 50 to 2,400. The proposed method maintains the highest accuracy across all dataset sizes and exhibits the steepest initial improvement, reaching 97.6% at 800 subjects and plateauing at 99.12% at 2,400 subjects. In contrast, the PCA-based baseline levels off below 91%, indicating an insufficient feature space dimensionality for large-scale identification. Presents a per-stage processing time breakdown for the proposed

method and the CNN-based baseline. The proposed pipeline completes end-to-end recognition in 115 ms, with the feature extraction stage (42 ms) and segmentation (35 ms) accounting for the majority of latency. The CNN baseline requires 180 ms in total, with feature extraction consuming 95 ms due to the forward-pass through a 24-layer network. Both methods meet the 300 ms threshold recommended by NIST for interactive access control applications. To assess cross-sensor and cross-domain generalisation, the proposed system was additionally tested on UBIRIS v2 and MMU2. Models trained exclusively on CASIA-IrisV4 and applied without fine-tuning to UBIRIS v2 (visible-spectrum, non-cooperative images) achieved a GAR of 91.4% and EER of 4.2%, reflecting the well-known domain gap between NIR and visible-spectrum iris images. When fine-tuned on 30% of UBIRIS v2 subjects, GAR improved to 95.7%, suggesting that the Gabor representation transfers reasonably across sensing modalities with modest adaptation. The results demonstrate that the proposed Gabor+SVM framework achieves superior biometric performance to both deep learning and classical machine learning baselines across all key metrics on CASIA-IrisV4. Several factors contribute to this outcome. First, multi-scale Gabor decomposition effectively captures the radially periodic and concentric texture structures characteristic of the iris, producing a compact yet highly discriminative 2,048-bit binary template. Second, the fractional Hamming distance—with its mathematically principled robustness to partial occlusion via noise masking—provides a reliable similarity score that the SVM ensemble refines by exploiting the full geometry of the feature space. The CNN baseline achieves slightly lower accuracy despite consuming 57% more processing time per query. This gap is consistent with findings in related literature [19, 20] and likely reflects two contributing factors: the relatively modest size of the training set (insufficient to leverage the full representational capacity of deep networks) and the absence of domain-specific inductive biases that Gabor-based encoding naturally encodes. We anticipate that the accuracy gap may narrow as training data volumes increase beyond 10,000 subjects, a direction that forms part of our ongoing work. The cross-dataset results reveal a non-trivial domain shift between NIR and visible-spectrum acquisitions. This finding underscores the practical importance of cross-spectral alignment techniques [22] or multi-spectral feature fusion strategies as directions for extending the current framework to unconstrained, at-a-distance deployment scenarios.

5. Conclusion

This paper presented a comprehensive iris recognition system grounded in Daugman's integro-differential operator for boundary localisation, rubber-sheet normalisation, multi-scale Gabor wavelet feature extraction, and a kernelised SVM classifier. The system achieved a Genuine Acceptance Rate of 99.12% and an Equal Error Rate of 0.44% on the CASIA-IrisV4 benchmark, surpassing CNN-based and LBP-based state-of-the-art methods while requiring significantly lower computational resources. The end-to-end latency of 115 ms on commodity CPU hardware confirms the system's readiness for real-time deployment in access control and identity management applications. Future research directions include: (i) integrating anti-spoofing liveness detection to guard against printed and artificial-eye presentation attacks; (ii) developing cross-spectral normalisation modules to bridge the performance gap between NIR-trained models and visible-spectrum deployments; (iii) adapting the pipeline for smartphone-based iris capture; and (iv) exploring federated learning approaches to enable privacy-preserving training across geographically distributed enrolment databases.

References

[1] Jain AK, Ross A, Prabhakar S (2004) An introduction to biometric recognition. IEEE Trans Circuits Syst Video Technol 14(1):4–20

[2] Bowyer KW, Hollingsworth K, Flynn PJ (2008) Image understanding for iris biometrics: a survey. Comput Vis Image Underst 110(2):281–307

[3] Daugman J (2004) How iris recognition works. IEEE Trans Circuits Syst Video Technol 14(1):21–30

[4] Wildes RP (1997) Iris recognition: an emerging biometric technology. Proc IEEE 85(9):1348–1363

[5] Ma L, Tan T, Wang Y, Zhang D (2004) Efficient iris recognition by characterizing key local variations. IEEE Trans Image Process 13(6):739–750

[6] Masek L, Kovesi P (2003) MATLAB source code for a biometric identification system based on iris patterns. Tech rep, The University of Western Australia

[7] Phillips PJ, Grother P, Micheals RJ (2002) Evaluation methods in biometric research. In: Biometric Systems, Technology, Design, and Performance Evaluation. Springer, London

[8] Daugman J (1993) High confidence visual recognition of persons by a test of statistical independence. IEEE Trans Pattern Anal Mach Intell 15(11):1148–1161

[9] Minaee S, Abdolrashidi A, Su H, Bennamoun M, Zhang D (2019) Iris recognition using scattering transform and textural features. In: EUSIPCO 2019. IEEE

[10] Lowe DG (2004) Distinctive image features from scale-invariant keypoints. Int J Comput Vis 60(2):91–110

[11] Boles WW, Boashash B (1998) A human identification technique using images of the iris and wavelet transform. IEEE Trans Signal Process 46(4):1185–1188

[12] Sun Z, Tan T (2009) Ordinal measures for iris recognition. IEEE Trans Pattern Anal Mach Intell 31(12):2211–2226
[13] Kumar A, Zhang D (2010) Personal recognition using hand shape and texture. IEEE Trans Image Process 15(8):2454–2461
[14] Tan CW, Kumar A (2012) Efficient and accurate at-a-distance iris recognition using geometric key-based iris encoding. IEEE Trans Inf Forensics Secur 9(6):1518–1526
[15] Nguyen K, Fookes C, Jillela R, Sridharan S, Ross A (2017) Long range iris recognition: a survey. Pattern Recognit 72:123–143
[16] Zhao Z, Kumar A (2017) Accurate periocular recognition under large pose variation using light CNN. IEEE Trans Inf Forensics Secur 13(5):1114–1126
[17] Gangwar A, Joshi A (2016) DeepIrisNet: deep iris representation with applications in iris recognition and cross-sensor iris recognition. In: ICIP 2016. IEEE
[18] Dosovitskiy A, Beyer L, Kolesnikov A et al (2021) An image is worth 16x16 words: transformers for image recognition at scale. In: ICLR 2021
[19] Ahmad T, Ahmad F, Ahmad I (2019) Iris recognition using multi-scale morphological gradient features. SN Appl Sci 1(12):1–12
[20] [20] Proença H, Filipe S, Santos R, Oliveira J, Alexandre LA (2010) The UBIRIS v2: a database of visible wavelength iris images captured on-the-move and at-a-distance. IEEE Trans Pattern Anal Mach Intell 32(8):1529–1535
[21] Chen X, An X, Yang W, Wu X (2021) An effective iris segmentation method using deep learning for iris recognition in non-cooperative environment. Symmetry 13(5):912
[22] Ramaiah NP, Kumar A (2017) Advancing cross-spectral iris recognition research using bi-spectral imaging. In: IJCB 2017. IEEE